2D Materials

RECEIVED
18 July 2016

REVISED
20 January 2017

ACCEPTED FOR PUBLICATION
27 January 2017

PUBLISHED
17 February 2017

PAPER

Electronic transport across metal-graphene edge contact

Cheng Gong[1,5], Chenxi Zhang[1], Young Jun Oh[1], Weichao Wang[1,2], Geunsik Lee[1,3], Bin Shan[1,4], Robert M Wallace[1] and Kyeongjae Cho[1,2]

[1] Department of Materials Science and Engineering, The University of Texas at Dallas, Richardson, TX 75080, United States of America
[2] Department of Electronics, Nankai University, Tianjin 300071, People's Republic of China
[3] Department of Chemistry, Ulsan National Institute of Science and Technology (UNIST), Ulsan 44919, South Korea
[4] Department of Materials Science and Engineering, Huazhong University of Science and Technology, Wuhan 430074, People's Republic of China
[5] Present address: NSF Nanoscale Science and Engineering Center (NSEC), 3112 Etcheverry Hall, University of California, Berkeley, CA 94720, United States of America

E-mail: kjcho@utdallas.edu

Keywords: metal-graphene, edge contact, electronic transport

Supplementary material for this article is available online

Abstract

The electronic transport across metal-graphene edge-contact structures is studied by first principles methods. Unusual double-dip transmission as a function of Fermi level is found for a Pd electrode over varying grapheme lengths. Interface metal-carbon hybridization is shown to introduce random distribution of π-orbital local density of states at different carbon sites leading to transmission suppression. For a Ti electrode, two dips are merged into one with a ~0.2 eV transport gap opening. Our work sheds light on the origin of intrinsic contact resistance at metal-graphene edge contact.

Graphene's electronic structure near the Dirac point is defined by the π-orbital band structure with a zero energy gap and linear energy-momentum dispersion [1]. The electronic transport property of a pristine graphene film is characterized by the conductivity (σ) as a function of gate voltage (V_g), which shows a V-shape with the conductivity minimum at the Dirac point [1]. Experimental studies have also shown that the Dirac point at nonzero V_g indicates that the graphene channel is uniformly doped by the ambient gas atmosphere, adatoms, chemical residues or dielectric substrates [2–4]. Through spatially controlled doping of graphene, a pn junction can be formed [5], and weakly interacting metal electrodes (e.g. Al, Au or Cu) dope graphene at the contact regions leading to n-i-n or p-i-p junctions [6–9]. The conductivities of such junctions are expected to have 'W-shape', with two minima (double dips) as a function of V_g, at the Dirac points of the graphene in contact and channel regions [5, 7].

A realistic metal-graphene (M-G) contact is beyond the description of the above simplified doping model, which only applies well for weakly interacting electrodes. However, such metals with low wettability do not bond well to graphene causing detaching problems, whereas metals with strong wettability are typically used in real devices (e.g. Pd, Ti/Au, Cr/Au, Ni and Co [10–13]). It has been well known that the strongly interacting electrodes destroy graphene's π-orbital band structure at the Dirac point [8]. Furthermore, the more serious effect is that carbon in graphene tends to react with deposited metals, making the metal's contact with the edge of an unreacted graphene channel [14, 15]. Therefore, the simple scenario of a metal contact with graphene surface does not suffice to account for the electronic transport in real graphene devices. In particular, Wang *et al* have developed controllable means to artificially fabricate metal-graphene edge contact, which exhibits much lower contact resistance compared with side contact [16]. Through *ab initio* quantum transport simulation, we show that there is still an intrinsic origin of contact resistance arising from the perturbation of graphene by the strong hybridization at the edge contact. The unusual double-dip transfer characteristic is demonstrated in a prototypical system of Pd-graphene edge contact, which has been frequently observed in experiments [10, 16], yet not been fully understood [5, 7, 17–24].

In this letter, a large-scale first-principles study of electronic transport across the M-G-M edge-contact structure is performed for commonly used Pd and Ti electrodes as representative systems. An unusual double-dip transmission characteristic is found in Pd-G-Pd: a fixed positive dip (at $E_F = 0.4$ eV) and a variable negative dip (at $E_F = -0.9 \sim -0.4$ eV depending on graphene channel length). Transmissions through the structures are suppressed by π-orbital local density of states (LDOS) variations among different carbon

sites perturbed by interface hybridization. In Ti/G/Ti end-contact structures, we found that a small transport gap forms [11, 25, 26]. It is worthwhile to note that the transport gap is not induced by a series of impurities in the vicinity of graphene [11] or Anderson localization due to edge disorder [25, 26], but by the electrode contact induced random potential scattering in the graphene. The contact resistance has been reported to be strongly affected by the interfacial hybridization between the metal d orbitals and the $p\pi$ orbitals of the graphene [27–29].

Calculation methods

The DFT calculations to optimize stable M-G edge-contact geometry are performed with the Vienna *ab initio* simulation package (VASP) [30] using the projected augmented wave potentials [31] and local density approximation. Metal's lattice sizes are strained (Pd stretched 3.2%, Ti compressed 3.7%) to match the graphene's periodic length 2.46 Å along zigzag edge, and the strain does not significantly change the electronic properties of the metals [10]. The optimized interfaces form strong metal-carbon bonding with 4.46 eV C^{-1} for Ti-G and 3.18 eV C^{-1} for Pd–G interfaces. Using the optimized edge-contact geometries, M-G-M structures are prepared for full quantum transport simulations using POSTRANS [32] which is a non-equilibrium Green's function program built on SIESTA DFT program. For the POSTRANS simulations, numerical atomic type orbital basis sets and Troullier–Martin type pseudopotentials [33] are used. We tested single-ζ, double-ζ and single-ζ polarized basis sets, which shows small differences around the Fermi level. Thus for the simplicity of our calculation, the single-ζ basis set is used for the electronic density matrix and transmission calculations. A cutoff energy of 150 Ry for the grid mesh is chosen.

Figures 1(a) and (c) show M-10G-M structures for M = Pd and Ti, where 10G indicates that the graphene channel has 10 units (each unit indicated by the yellow box) along the transport z direction. Green boxes represent semi-infinite metal electrodes, and the red boxes represent the supercells along the transverse y direction. Therefore, in this study the electronic transport is directly modeled from metal electrodes into the graphene channel in contrast to the previous side-contact study [5, 7, 24] in which metal-to-graphene charge transport was not directly studied as a metal-graphene complex was modelled as an electrode.

Double-dips transmission characteristic of Pd-*n*G-Pd

Figure 1(b) shows a transmission as a function of Fermi level (E_f) which is different from the commonly reported V-shape conductivity curve as a function of V_g. Several features are observed in the transmission characteristics of Pd-nG-Pd illustrated in figure 1(b): (1) In each curve, there are two transmission dips within ± 1 eV with respect to the Fermi level; (2) All curves have a common positive dip ('$+D$') at around 0.4 eV above the Fermi level, but negative dips ('$-D$s') appear at different positions; (3) the transmission at the $+D$s are suppressed to be vanishing, but those at the $-D$s are partially suppressed depending on graphene length.

Feature (2) discloses a fixed position of $+D$ which indicates that the $+D$'s origin likely arises from a doping effect of contacts. To examine the detailed electronic structure changes at the Pd-G interface and their effects on the electronic transport across Pd-G interface, we have carried out a detailed LDOS analysis of both A and B sub-lattice carbon atoms as a function of the distance from the interface. From these LDOS plots, it is not easy to identify the Dirac point (i.e. zero DOS point) due to the presence of hybridized states, but one can use the DOS peak (−2.4 eV for intrinsic graphene shown in figure 2(b) bottom) as a guide to estimate that the location of the 'Dirac point' is ~0.4 eV above the Fermi level. Near the interface, graphene is thus ~0.4 eV p-type doped by Pd in agreement with its large work function of 5.56 eV [8]. Figure 2(b) also shows that graphene does not recover an intrinsic DOS even in the middle of the 10G graphene channel, and in agreement with the known long-range character of doping effect [34]. This analysis confirms that the transmission dip at 0.4 eV is a result of doped graphene by Pd contact. However, the transmission dip at negative E_F is not expected and the DOS plots in figures 2(a) and (b) do not show obvious features explaining the large suppression of transmission close to $-D$s.

The negative transmission dip (figure 1(b)) can be explained by LDOS variations in graphene caused by interface hybridization. Figure 2(c) top panel shows the transmission of Pd-10G-Pd structure over the energy range of $-1.0 < E_F < -0.05$ eV, and the bottom panel shows the average and the standard deviation of LDOS calculated over 80 carbon atomic sites as a function of energy. Figure 2(c) bottom panel also summarizes the ratio of standard deviation over the average value (DAR = dev./avg.).

In the region I, the LDOS deviation (green curve) stays constant and the average (blue curve) decreases as the energy increases. This increase in DAR (black curve, from 0.2 to 0.5) indicates a reduced electron transmission probability (red curve). In this region, the DOS profile does not show significant barrier/well formation (see figure 3(d)). In stark contrast, the region II shows much larger DAR (close to 1), representing a highly fluctuating LDOS. As seen from figure 3(a), the carbon π-orbital DOS has a highly non-uniform distribution (see figure 3(a)) so that the carrier transmission throughout the graphene channel may even be pinched off, where the transmission dip is produced. In the region III, the average gradually increases and the deviation decreases. Consequently, the DAR decreases agreeing with the increased transmission. In the region IV, the average and deviation of the LDOS remain constant, and the DAR also remains constant agreeing with a constant transmission. The analysis based on the DAR

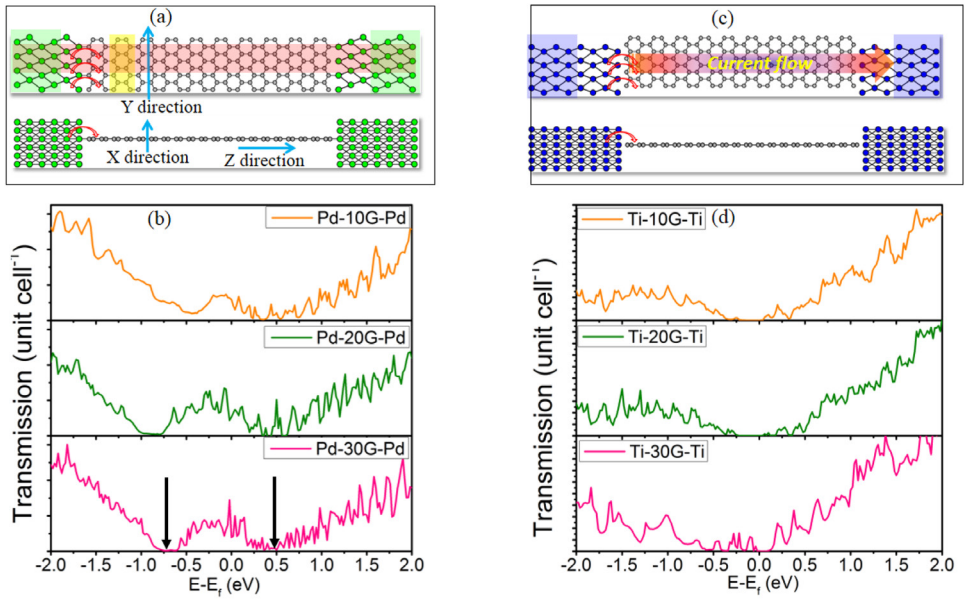

Figure 1. Top and side views of (a) Pd-10G-Pd and (c) Ti-10G-Ti structures. Transmission versus energy of (b) Pd-*n*G-Pd and (d) Ti-*n*G-Ti ($n = 10, 20$, and 30). Periodic boundary condition is applied along *X* and *Y* directions. The equilibrium interface distance between bottom carbon atoms and metal surfaces are 1.72 Å (Pd), and 1.58 Å (Ti). Two vertical solid black arrows point to the positions of two dips for Pd-30G-Pd. The longest channel reaches the regime of realistic nanoscale devices at 12.78 nm ($n = 30$).

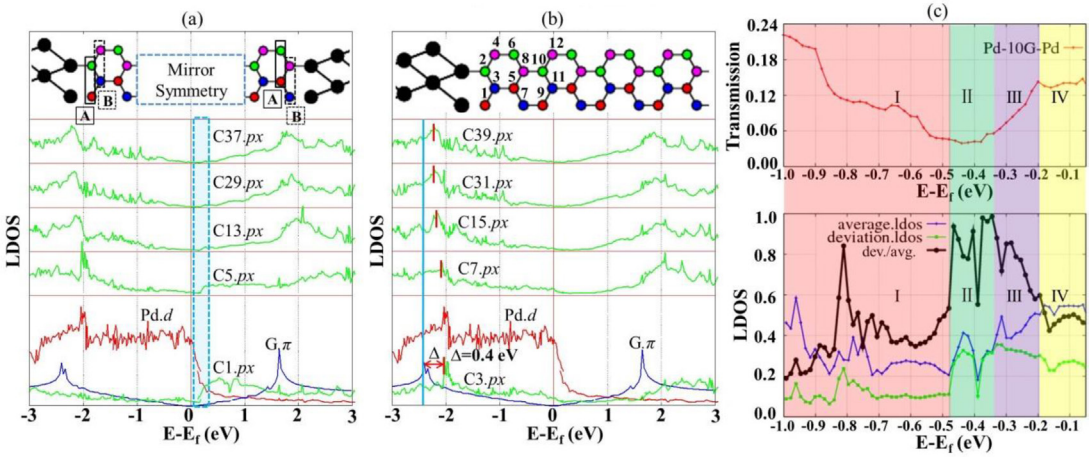

Figure 2. LDOS of sampled carbon atoms on (a) A and (b) B sub-lattices. The intensity of Pd *d*-orbital DOS is 1/30 offset. The rectangular box in (a) indicates the Pd-C electronic state hybridization of A sub-lattice in contrast to the absence of such states in the B sub-lattice DOS in (b). Upper figure of (c) is the transmission of Pd-10G-Pd at $[-1.0, -0.05]$ eV, and the below figure is the LDOS fluctuation analysis.

of LDOS provides a quantitative measure of the transmission behavior around the negative dip, confirming the hybridization induced scattering centers as the origin of suppressed transmission for negative dips.

On the one hand, strong interfacial hybridization with a short metal-carbon bonding length (<2 Å) eliminate the tunneling barrier for electron injection across metal-graphene side-contact interfaces (>3 Å) [8, 35]. One the other hand, the strong interfacial metal-carbon bonding destroys graphene's uniform π-conjugations, creating random scattering centers. Figure 4 confirms that graphene's electronic wave function is substantially disturbed by Pd contact. In the language of the tight binding scheme, nonuniform charge distribution (illustrated in figures 4(b) and (c)) is a direct reflection of non-uniform carbon on-site potentials. Furthermore, the nonuniform bonding charge density connecting neighboring C–C atoms (illustrated in figure 4(a)) describes variable bonding strengths, which implies variable charge hopping efficiencies. This analysis shows the importance and necessity of the first prinicples study (compared to a TB model) to include the detailed electronic structure changes in graphene transport study.

Ti-*n*G-Ti electronic transport

Unlike Pd-G-Pd with double-dip transmission, Ti-G-Ti shows a small transport gap (~0.2 eV) near the Dirac point in figure 1(d). The transmission shows a

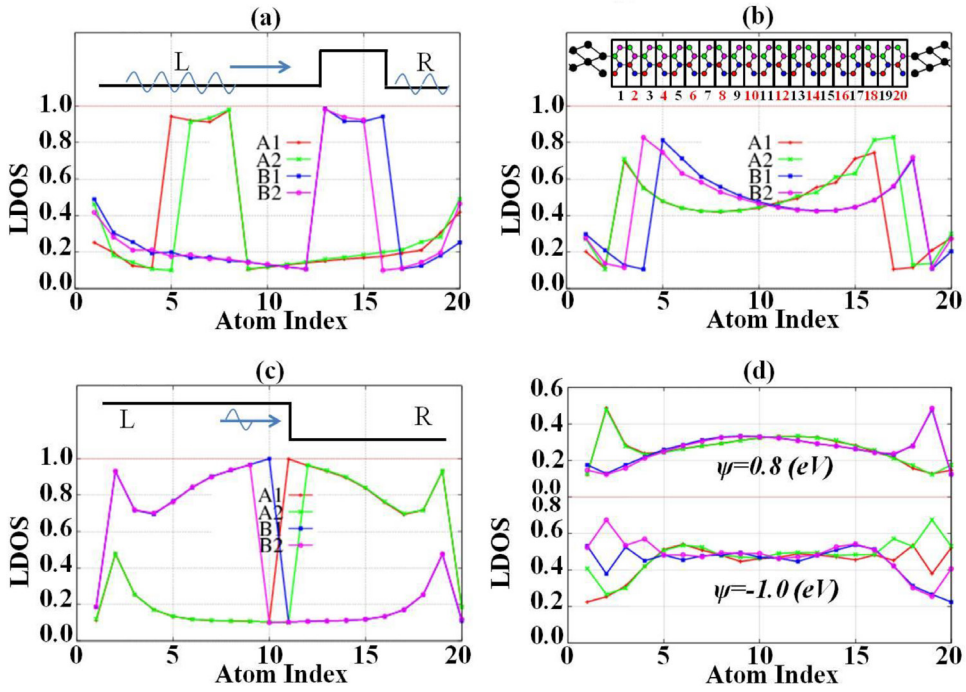

Figure 3. π-orbital LDOS profiles at energy of (a) -0.4 eV, (b) 0.0 eV, (c) 0.4 eV and (d) 0.8 eV and -1.0 eV along the whole channel. Top panel of (b) shows the atomic index 1–20 where each index contains two A sub-lattice atoms (A1 and A2) and B sub-lattice atoms (B1 and B2). Top panels of (a) and (c) show the sketches of LDOS of B sub-lattice atoms.

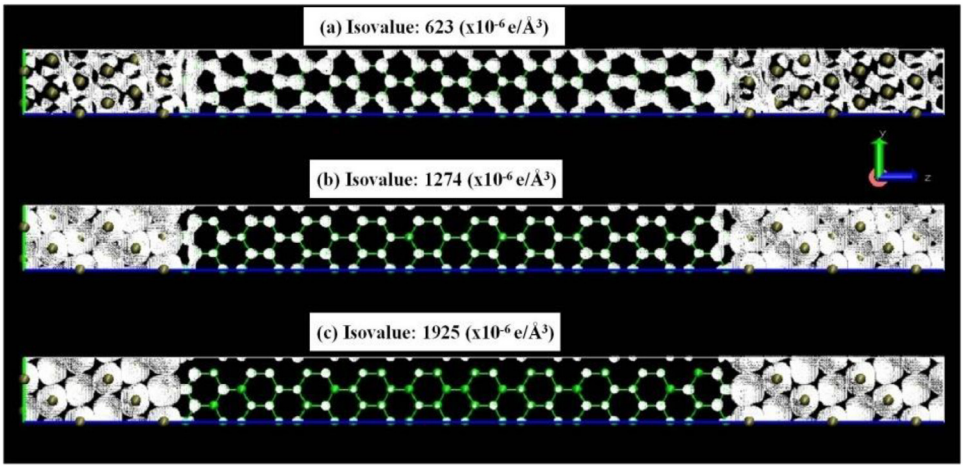

Figure 4. Total charge density distribution contour plots at three different isovalues: 623, 1274, and 1925 ($\times 10^{-6}$ e Å^{-3}) for Pd-10G-Pd structure in figure 1(a). The small isovalue clearly shows carbon electron density and bonding distributions. The large isovalues clearly show Pd electron density and Pd-C interface bonding charges.

strong asymmetry, which can be explained by the *n*-type doping of the graphene by Ti electrode and the partially occupied *d*-band of Ti electrode that has asymmetric density of states (DOS) around Fermi level. (See details in figure S5 in the supplementary information (stacks.iop.org/TDM/4/025033/mmedia)) Stronger interfacial hybridization suppressed the transmission near Fermi level, resulting in a transport gap as shown in figure 1(d). (See details in figures S4 and S7 in the supplementary information) This simulation result qualitatively agrees with the experimental finding that the transport gap does not have a strong dependence on graphene length [11].

In summary, the electronic transport across hybridized metal-graphene interface is studied based on metal-graphene-metal edge-contact structures. Although the shorter interfacial metal-carbon bonding length at edge contact eliminates the interfacial tunneling barrier present in side-contact interfaces, the strong interfacial hybridization disturbs the uniform graphene channel and results in scattering centers. Our work not only reveals in detail the electronic transport behaviors at metal-graphene edge contact, but also sheds light on the intrinsic origin of contact resistance at this novel contact geometry.

Acknowledgments

We thank Professor K W Kim for the sharing of the POSTRANS program. We acknowledge Prof William G Vandenberghe, Dr Roberto C Longo Pazos, Dr Chaoping Liang and Bo Ma for their helpful discussions. This work was supported by the Creative Materials Discovery Program on Creative Multilevel Research Center (2015M3D1A1068062) through the National Research Foundation (NRF) of Korea funded by the Ministry of Science, ICT & Future Planning. This work was also partially supported by National Natural Science Foundation of China (11304161) and Start-up Research Grants from Nankai University.

References

[1] Novoselov K S *et al* 2004 *Science* **306** 666
[2] Schedin F *et al* 2007 *Nat. Mater.* **6** 652
[3] Chen J-H *et al* 2008 *Nat. Phys.* **4** 377
[4] Emtsev K V *et al* 2009 *Nat. Mater.* **8** 203
[5] Maassen J, Ji W and Guo H 2010 *Appl. Phys. Lett.* **97** 142105
[6] Giovannetti G *et al* 2009 *Phys. Rev. Lett.* **101** 026803
Khomyakov P A *et al* 2009 *Phys. Rev.* B **79** 195425
[7] Barraza-Lopez S *et al* 2010 *Phys. Rev. Lett.* **104** 076807
[8] Gong C *et al* 2010 *J. Appl. Phys.* **108** 123711
[9] Gong C *et al* 2012 *ACS Nano* **6** 5381–7
[10] Poumirol J-M *et al* 2010 *Phys. Rev.* B **82** 041413
[11] GallagherP, Todd K and Goldhaber-Gordon D 2010 *Phys. Rev.* B **81** 115409
[12] Venugopal A, Colombo L and Vogel E M 2010 *Appl. Phys. Lett.* **96** 013512
[13] Nouchi R, Shiraishi M and Suzuki Y 2008 *Appl. Phys. Lett.* **93** 152104
[14] Gong C *et al* 2013 *ACS Nano* **8** 642–9
[15] Zan R, Bangert U, Ramasse Q and Novoselov K S 2011 *Nano Lett.* **11** 1087–92
[16] Wang L *et al* 2013 *Science* **342** 6158
[17] Gao Q and Guo J 2014 *APL Mater.* **2** 056105
[18] Low T *et al* 2009 *IEEE Trans. Electron Devices* **56** 6
[19] Blanter Y M and Martin I 2007 *Phys. Rev.* B **76** 155433
[20] Robinson J P and Schomerus H 2007 *Phys. Rev.* B **76** 115430
[21] Nemec N, Tománek D and Cuniberti G 2006 *Phys. Rev. Lett.* **96** 076802
Nemec N, Tománek D and Cuniberti G 2008 *Phys. Rev.* B **77** 125420
[22] Golizadeh-Mojarad R and Datta S 2009 *Phys. Rev.* B **79** 085410
[23] Matsuda Y, Deng W-Q and Goddard W A III 2011 *J. Phys. Chem.* C **114** 17845
[24] Barraza-Lopez S, Kindermann M and Chou M Y 2012 *Nano Lett.* **12** 3424
[25] Evaldsson M *et al* 2008 *Phys. Rev.* B **78** 161407
[26] Mucciolo E R, Castro Neto A H and Lewenkopf C H 2009 *Phys. Rev.* B **79** 075407
[27] Stokbro K, Engelund M and Blom A 2012 *Phys. Rev.* B **85** 165442
[28] Cho Y, Choi Y C and Kim K S 2011 *J. Phys. Chem.* C **115** 6019
[29] Liu H, Kondo H and Ohno T 2012 *Phys. Rev.* B **86** 155434
[30] Kresse G and Furthemüller J 1996 *Comput. Mater. Sci.* **6** 15
[31] Blöchl P E 1994 *Phys. Rev.* B **50** 17953–79
[32] Kim W Y and Kim K S 2008 *J. Comput. Chem.* **29** 1073
[33] Soler J M *et al* 2002 *J. Phys.: Condens. Matter* **14** 2745
[34] Khomyakov P A *et al* 2010 *Phys. Rev.* B **82** 115437
[35] Shan B and Cho K 2004 *Phys. Rev.* B **70** 233405